

# Bionanocomposites reinforced with cellulose fibers and agro-industrial wastes

18

Swati Chaturvedi<sup>a</sup>, Aditya Kataria<sup>a</sup>, Vaibhav Chaudhary<sup>a</sup>, Akarsh Verma<sup>a,b</sup>, Naman Jain<sup>c</sup>, Mavinkere Rangappa Sanjay<sup>d</sup>, and Suchart Siengchin<sup>d</sup>

<sup>a</sup>Department of Mechanical Engineering, University of Petroleum and Energy Studies, Dehradun, Uttarakhand, India, <sup>b</sup>Brigham Young University, Provo, UT, United States,

<sup>c</sup>Department of Mechanical Engineering, ABES Engineering College, Ghaziabad, India,

<sup>d</sup>Department of Materials and Production Engineering, The Sirindhorn International Thai-German Graduate School of Engineering (TGGS), King Mongkut's University of Technology North Bangkok, Bangkok, Thailand

## 18.1 Introduction

Cellulose is a homopolysaccharide that has glucose-glucose linkages. These linkages are arranged in linear chains. Cellulose has many properties like it is easily available, is biocompatible and biodegradable, and many more properties. Cellulose nanofibers have many unique characteristics like good mechanical properties such as high tensile strength, formation of highly porous mesh, high Young's modulus, large surface-to-volume ratio, and high surface area (Rani, Monga, Bansal, & Sharma, 2018). Due to the formation of hydrogen bonds and mechanical interlocking between the fibers of extracted cellulose nanofibers, a web-like structure is formed which possess a high aspect ratio. Mechanical properties are boosted by nano-reinforced polymer composites to a great extent. Thus, they are of great importance. Researchers who are in automation, construction, and aerospace field are attracted toward the natural fiber-reinforced composites due to its eco-friendly characteristics and lightweight nature (Siva et al., 2020). Properties of matrix and filler, interaction between them and quality of filler that is dispersed inside the matrix are some of the factors that determine the mechanical properties (Verma, Jain, Rangappa, Siengchin, & Jawaid, 2021).

Various factors including thermal properties decide the use of cellulose bionanocomposites. For the production of papers that are thermally insulated and for producing insulating material for electrical appliance, cotton stalk fibers and hemp fibers are used. High thermal insulating properties are possessed by biocomposites, which are produced from silica and chitosan. Various factors such as moisture condition, interaction of hydroxyl group are present on cellulose surface with other molecules (Zia, Jabeen, Anjum, & Ikram, 2020). Biocomposites are generally used for applications where the temperature required is higher than the normal room temperature. To know the thermal stability of composites before using them, TGA is used. It gives us insight about degradation temperature of the bionanocomposites. Most of the

biocomposites degraded in two steps. Weight loss is studied in first step. Decomposition and degradation of fibers are studied in the second stage (Guleria, Singha, & Rana, 2017).

## 18.2 Mechanical properties

### 18.2.1 Natural rubber-based composites

When cellulose nanofiber content was increased to 2 phr, the tensile strength of natural rubber-cellulose nanocomposite increased because the formation of zinc/cellulose nanofiber (Zn/CNF) and fiber-fiber network takes place, and percolation of fiber-matrix interaction will be there. The tensile strength decreased when 4 phr of cellulose nanofiber content was added. This is because agglomeration of fibers takes place when high fiber loading is there; as a result, formation of bundles takes place due to which fiber-fiber interaction supercedes fiber-matrix interaction. Due to this formation of voids takes place, which are centers of stress concentration. The tensile strength of the natural rubber decreased because adhesion forces between fiber that was hydrophilic and polymer matrix that was hydrophobic were poor. There was decrease in elongation of natural rubber-cellulose nanofiber composite when cellulose nanofiber content was increased. This decrease was due to decrease in mobility of the polymer chains due to addition of cellulose nanofibers (Midhun Dominic et al., 2020). The modulus improves up to 3 phr cellulose nanofiber content addition at 300% elongation. This increase was due to the immobilization of polymer chains due to the formation of three-dimensional networks of Zn/CNF and fiber-fiber. When CNF loading increased, modulus decreased. This decrease was due to fiber agglomeration. Another reason for this decrease in modulus was less cross-link density. The tear strength increased at 2 phr cellulose nanofiber content loading, because obstruction was created to the tear path by cellulose nanofiber content in the longitudinal direction; and due to its homogeneous dispersion and proper orientation, nanofibers could effectively resist the propagation of crack. However, at 4 phr of cellulose nanofiber content loading, the tear strength decreased due to fiber agglomeration. The hardness of the composite increased when cellulose nanofiber content was increased. This is because stiffness of the composite increased due to reduction in mobility of matrix (Midhun Dominic et al., 2020). Buckling happens when fibers are compressed in the direction in which they are aligned due to which compression set values increases as we increase the content of cellulose nanofiber content. The number of buckling decreases due to mercerization and latex stage processing. This increases the interaction between fiber and matrix. As a result, compression set value decreases at lower loading of cellulose nanofibers (Midhun Dominic et al., 2020). Due to uniformity in dispersion and correct orientation, less dissipation of energy will take place at interface of the fiber and matrix. As a result, rebound resilience of nanocomposite would increase. The abrasion index for nanocomposite is maximum when content of cellulose nanofiber content is 2 phr, this is because of the good fiber-matrix interaction (Midhun Dominic et al., 2020). Due to weak interfacial adhesion between the

cellulose nanofiber and natural rubber matrix, pulling out of fibers also happens that degrades the properties of the resulting nanocomposites (Kumagai et al., 2019).

### **18.2.2 Polyvinyl alcohol (PVA) matrix-based composites**

Nuruddin et al. (Nuruddin, Gupta, Tcherbi-Narteh, Hosur, & Jeelani, 2015) reported that the tensile modulus of the PVA improved on adding small amount of nanofibers in composite sample. This increase was due to the formation of strong hydrogen bonds that takes place between nanofibers of cellulose and polyvinyl alcohol. As a result, the matrix dispersion of nanofibers takes place and superior load transfer takes place from the matrix to reinforcement. When cellulose nanofiber content was increased up to 5%, tensile strength of nanocomposite improved by 41%–49% and elastic modulus increased by 258%–267%. The reason for this increase was the increase in the formation of hydrogen bonding between fiber and polymer. The mechanical properties decreased due to agglomeration formation into PVA matrix system (Nuruddin et al., 2015).

### **18.2.3 Epoxy resin matrix-based composites**

Kurita et al. (Kurita, Ishigami, Wu, & Narita, 2021) reported that on addition of cellulose nanofibers to the epoxy-cellulose nanofiber content composites, the Young's modulus was found to increase while the fracture elongation decreased. This showed that there was a transition in epoxy composites from ductile to brittle. Due to the stiff nature of the agglomerated cellulose nanofiber clusters, epoxy cellulose nano fiber content composites became harder than the neat epoxy resin. As a result, 1.8 vol% of epoxy cellulose nano fiber content composites crushed and there was deflection in the neat epoxy (Kurita et al., 2021). When the percentage of volume fraction of cellulose nanofibers was up to 2.0, the ultimate tensile strength and ultimate flexural strength of the epoxy cellulose nanofiber composites increased. On the other hand, when the volume percentage was increased to 2.2, the ultimate tensile strength and ultimate flexural strength of the epoxy-cellulose nanofiber content composites decreased. The reason behind this was the increased fiber-to-fiber interaction in the matrix, due to which coarse cellulose nanofiber agglomeration created the concentration of stress in the epoxy cellulose nanofibers composites (Kurita et al., 2021). It was noted that due to chemical interaction between epoxy resin and cellulose nanofiber, mechanical properties of epoxy resin enhanced when the volume fraction of cellulose nanofiber was less. Epoxy-cellulose nanofiber content composites strengthening mechanism showed different behavior at different values of volume fraction of cellulose nanofiber (Kurita et al., 2021).

Nissilä et al. (Nissilä, Hietala, & Oksman, 2019) reported that the tensile and flexural moduli increased by 30% and 74%, when 13% cellulose nanofiber content was added by volume. This was due to increase in stiffness of the material. Stiffness increased because a network like cellulose nanofiber content reinforcement was formed by aerogel inside the matrix. The structure of the network was anisotropic because there were differences in the longitudinal and transverse moduli.

The longitudinal strength was unaffected when the vol% was 10, but increased when the vol% was 13. The reason behind this increase was the difference in the void content. Also, the composite became fragile in the transverse direction, due to the weak interfacial adhesion along with alternating epoxy/cellulose nanofiber content structure (Nissilä et al., 2019). Due to increase in number of clumping and agglomerations, poor dispersion of the cellulose nanofiber takes place in the epoxy matrix. Thus, mechanical properties reduce when the content of cellulose nanofiber was 1% (Saba et al., 2017).

### **18.2.4 High-density polyethylene (HDPE)-based composites**

Mulinari et al. (Mulinari, Voorwald, Cioffi, & da Silva, 2017) examined that the mechanical properties got changed when cellulose fibers were added to the high-density polyethylene matrix. The Young's modulus increased more than two times from a value of 732.5 to 1629 MPa, when the fiber content was increased to 40 wt%. This increase took place due to the modifications in the fiber. As a result of modification in the fiber, interaction with the polymer matrix increased due to the decrease in the interfacial tension between fiber and polymer chains. There was decrease in elongation at break. At the interface of the fiber and matrix, deformability reduced which resulted in the decrease of the elongation of composites (Mulinari et al., 2017). Number of fibers reinforced in the matrix also had an impact on the flexural properties such as flexural modulus and flexural strength of the composites. The flexural modulus increased from 0 wt% to 40 wt%. Due to the compressive stresses which were developed in the transverse section of the flexural specimens during bending, better interaction between fiber and matrix takes place. This better interaction increases the flexural modulus of composites. The author reported that the impact strength also increased. When fibers were inserted in the matrix, there was an increase in absorbed energy, which was due to the limitations on the plastic nature of the composites as the fibers were brittle in nature. Eventually, strength also got increased due to the energy dissipation mechanism. During the mechanical process, energy got dissipated and the fibers were pulled out (Mulinari et al., 2017).

### **18.2.5 Poly butylene succinate (PBS)-based composites**

In 2016, Joy et al. (Joy et al., 2016) reported that the toughness of poly butylene succinate nanocomposites reinforced with cellulose nanofibers was less as compared to the pure poly butylene succinate. This decrease was due to the cellulose nanofibers particles, which acted as stress concentrators. Modulus of resilience of the poly butylene succinate composites reinforced with cellulose fibers increased up to the loading level of 1.5 phr. This increase was due to the increase in interfacial interaction between fibers and matrix. On the other hand, when the concentration of cellulose fibers was increased, the value of strain at break decreased because of the restriction offered by cellulose nanofibers increased. The value of Young's modulus increased when the content of cellulose nanofibers was increased from 3.8 to 4.9 GPa. This reason behind this increase was enhancement in restriction by cellulose nanofiber to chains of polymer. Cellulose nanofibers formed network with the help of hydrogen bonding

interaction in the poly butylene succinate matrix as a result, the mobility of the PBS chains decreased (Joy et al., 2016).

### **18.2.6 Starch-based composites**

The value of tensile strength increased from 1.64 times when eucalyptus nanocellulose was added into starch matrix (Almeida et al., 2020). The reason behind this was the improvement in dispersion within the starch matrix and formation of hydrogen bonds between starch and nanocellulose. On the other hand, when the percentage of nanocellulose was increased to 1.5%, decrease in the tensile strength was noticed. The reason behind this decrease was the formation of discontinuous and heterogeneous phase from the aggregation of nanocellulose (Almeida et al., 2020).

### **18.2.7 Polyethylene oxide (PEO)-based composites**

Tensile strength increased when cellulose nanofibers were reinforced in poly(ethylene oxide) (Safdari, Carreau, Heuzey, Kamal, & Sain, 2017). The reason behind this increment was good interaction between the polymer matrix and cellulose nanofibers that increased the transfer of stress from matrix to the fibers. The network of strong fibers also enhanced transferring of load. Elongation at break decreased when cellulose nanofibers were loaded; due to the reduction caused in the mobility of chains in the presence of filler. There was no change noticed in the values of Young modulus and tensile strength when it was prepared in the molten state. The reason behind this was creation of large agglomerations and very less quantity of cellulose nanofiber presence (Safdari, Carreau, Heuzey, Kamal, & Sain, 2017).

### **18.2.8 Polyacrylamide (PAM)-based composites**

When 5 wt% was added in pure polyacrylamide (PAM), the value of fracture strain increased 1.22 times (Chen, Wang, Li, Fang, & Li, 2017). The reason behind this was that the cellulose nanofiber got well dispersed in the matrix. Cellulose nanofiber property of large aspect ratio helped them to form network structure inside the poly acrylamide matrix. The force transferred from matrix to fibers and fibers to fibers improved because of the formation of network, as a result, mechanical properties improved. Formation of hydrogen bond between cellulose nanofibers and polyacrylamide, and dispersion of cellulose nanofibers in the polyacrylamide matrix leading to the formation of network were the main mechanism behind toughening effect (Chen et al., 2017).

### **18.2.9 Polystyrene (PS)-based composites**

The authors (Neves, Lopes, Zimmermann, Poletto, & Zattera, 2019) reported when cellulose nanofibers were added, it led to the hardening of the composite. The reason behind this was increased interaction between cellulose nanofibers and PS matrix, because of the large surface area of cellulose nanofibers. When the content of

cellulose nanofibers was 1%, highest value of modulus was noticed. The reason behind this was uniformity in dispersion of this concentration (Neves et al., 2019).

### **18.2.10 Poly(lactic acid)-based composites**

The authors (Wang & Drzal, 2012) reported that the value of modulus and strength of PLA increased 1.57 times. The reason behind this increase was strong web-like structure of cellulose nanofiber. Another reason was high aspect ratio of cellulose nanofibers. The strain at break of PLA also increased when cellulose nanofibers were added. The reason behind this increase was due to the agglomeration of cellulose in poly(lactic acid) matrix (Wang & Drzal, 2012).

## **18.3 Thermal properties**

### **18.3.1 Natural rubber-based composites**

In the literature (Almeida et al., 2020), the thermal properties of cellulose fiber and natural rubber degraded when cross-linking agents were added (except when the filler concentration was 1% of cellulose fiber). This degradation was due to the lower thermal stability of cellulose fiber. But, when the concentration of filler was less, formation of hydrogen bonding took place natural rubber and cellulose fiber, which contributed in the improvement of thermal properties. At lower filler content, thermal stability of the nanocomposites increased. The reason of this increase was presence of percolation network; zinc/cellulose complex and latex phase have homogenous distribution of fillers in it. When the loading of filler was high, then decomposition temperature decreased which was mainly due to the three reasons—critical volume fraction, agglomeration when the concentration was high, and percolation threshold. At higher weight percentages, agglomeration of particles took place due to the surface polarity of nano cellulose, which was due to the hydroxyl group. The early temperature degradation is also enhanced by the oxygen, which are present in the backbone and side chains of cellulose. As the percentage of nanocellulose is increased, active centers, which were created for the interaction with filler starts decreasing as the tendency of rubber to create them decreases, and filler-filler interaction increases (Almeida et al., 2020).

### **18.3.2 Epoxy-based composites**

Weight loss as a function of temperature is used for determining the thermal stability of specimens using thermogravimetric analysis (TGA). When neat epoxy was present, the thermal parameters were lower as compared to the cellulose-based composite (Guleria et al., 2017). The reason behind this was that cellulose from the atmosphere attracts water. Two distinct stages of decomposition were shown by epoxy and nanocellulose-based composites, which can be seen from TGA curves reported in the reference number 10. At 375°C, thermal degradation's first step started, which

was related to the moisture vaporization, which was present in composite. Second stage included the degradation of epoxy and nanocellulose additives. When additives were added, the TGA curve shifted to higher temperatures. The reason behind this shift was increased interaction between the nanocellulose and epoxy matrix. The heat transfer was prevented by nanocellulose to the epoxy matrix. Nanocellulose also acted as a barrier to the volatile material, which was produced during decomposition of epoxy matrix (Guleria et al., 2017).

### **18.3.3 Polyvinyl alcohol-based composites**

The thermal stability of composites with matrices of thermoplastic usually reduces upon inclusion of cellulosic reinforcement (Ramezani Kakroodi, Cheng, Sain, & Asiri, 2014). The degradation temperature increased when cellulose nanofibers were included. The reason behind this behavior was thermal stability of nanofiber, which was high due to the separation of components such as lignin; and hemicellulose, which were less stable. Another reason of this behavior was due to the homogeneous distribution of cellulose nanofibers in the matrix, and the mobility of the polymer chains in polyvinyl alcohol was restricted (Ramezani Kakroodi et al., 2014).

### **18.3.4 Poly ethylene-co-vinyl acetate (EVA)-based composites**

The value of glass transition temperature ( $T_g$ ) increased by the incorporation of bacterial cellulose nanofibers to poly ethylene-co-vinyl acetate (EVA) (Ghadikolaie, Omrani, & Ehsani, 2018). The reason behind this was the increase in mobility, which took place in nanocomposite domain and rubbery nature. However, there was decrease in the enthalpy values. However, decrease was noticed in enthalpy of melting and crystallinity percentage when bacterial cellulose nanofibers were incorporated in poly ethylene-co-vinyl acetate. The reason for this decrease was the alteration caused to the crystallinity of the nanocomposite because of the partly amorphous bacterial cellulose nanofibers. But, when acetylated bacterial monocellulose was used, increase in enthalpy of melting and crystallinity percentage was noticed. The reason behind this increase was better compatibility of the acetylated bacterial cellulose nanofibers with poly ethylene-co-vinyl acetate polymer and good interfacial adhesion between them (Ghadikolaie et al., 2018).

### **18.3.5 Poly(3-hydroxybutyrate) (PHB)-based composites**

When the concentration of cellulose fibers (CF) was increased, the thermal stability of poly(3-hydroxybutyrate) increases (Panaitescu, Nicolae, Gabor, & Trusca, 2020). The reason behind this was the increase in shear that took place during melt processing. The value of crystallinity was high for PHB/CF composites as compared to the PHB reference. The reason for this was nucleating effect of cellulose fiber. The value of  $T_g$  was also high for composites as compared to that of poly(3-hydroxybutyrate) reference. Increased interaction between cellulose fiber and poly(3-hydroxybutyrate)

matrix and reduction in mobility of poly(3-hydroxybutyrate) chains close to cellulose fiber were the chief reasons. If amount of plasticizer is doubled, value of glass transition temperature decreased. The reason behind this was increase in mobility of poly(3-hydroxybutyrate) chains, which was induced by plasticizer (Panaitescu et al., 2020).

### **18.3.6 Polypropylene-based composites**

Two degradation stages were shown by thermogravimetric (TG) curves (Luz, Del Tio, Rocha, Gonçalves, & Del'Arco Jr, 2008). Between 30°C and 100°C, the first stage of weight loss occurred. This loss was due to the water vaporization heat present in the sample. When fibers/PP composites are produced, significant level of water is released by cellulosic fibers. This released was because the fibers need to be dried before processing. The second stage of weight loss occurred of the cleavage of chemical bonds of glucosidic linkages, which were present in cellulose. Formation of aromatic compound took place at around 350°C. While at around 400–500°C, 88% of ashes were produced by cellulose, which mainly consisted of polycyclic aromatic compound (Luz et al., 2008).

### **18.3.7 Polyurethane-based composites**

When the wt% of cellulose nanofiber was increased to 2% from 0.5%, the value of  $T_g$  of the nanocomposite increased (Ivdre, Mucci, Stefani, Aranguren, & Cabulis, 2016). This increase was due to increased interaction between the fiber and matrix. Second, the association between cellulose and polyurethane (PU) matrix's soft segment was increased and grew stronger which restricted the molecular mobility. The degree of crystallinity decreased as the content of nanocellulose was increased. The reason behind this restriction caused to the growth of cellulose nanofiber-based polyurethane due to the presence of cellulosic network, which was highly developed. Another reason behind this increase was that matrix cellulose interaction increased through physical bonding with the help of hydroxyl groups that were present on the surface cellulose nanofibers. Good thermodynamic compatibility between cellulose nanofiber and polyurethane was also the reason behind this increase (Ivdre et al., 2016).

### **18.3.8 Xylan-based composites**

The author (Abdulkhani, Mazhar, Hedjazi, & Hamzeh, 2019) reported increase in onset temperature upon incorporation of xylan with oxidized carboxymethyl cellulose. The reason behind this increase in thermal stability of biocomposite upon reinforcement with oxidized carboxymethyl cellulose was the formation of hydrogen bonds and restriction in mobility of chains.



### **18.3.9 Poly(ethylene glycol)-based composites**

The crystallinity increases when poly(ethylene glycol) is added to polylactide (Safdari, Carreau, Heuzey, & Kamal, 2017). The reason behind this increase was the increase in mobility of polymer chains due to the poly(ethylene glycol) role of plasticization. The value of  $T_g$  increased. This is because on the crystallization of PLA, synergistic effect of poly(ethylene glycol) and cellulose nanofiber is caused (Safdari, Carreau, Heuzey, & Kamal, 2017).

### **18.3.10 Starch-based composites**

The glass transition temperature of thermoplastic starch matrix increased when cellulose nanofibers were added into it (Ghanbari, Tabarsa, Ashori, Shakeri, & Mashkour, 2018). The reason behind this increase was reduction in the flexibility of the polymeric chains due to the strong interaction that took place between hydroxyl groups of cellulose nanofibers with thermoplastic starch. Another reason behind this was nucleating effect of cellulose nanofiber on the thermoplastic starch matrix. Factors like cellulose-water interaction, reduction in matrix mobility due to strong interaction between matrix and cellulose nanofibers because of the presence of hydroxyl group, and selective partitioning of glycerol were responsible for increase in transition temperature when cellulose nanofibers were added (Pelissari, Andrade-Mahecha, do Amaral Sobral, & Menegalli, 2017).

## **18.4 Fabrication processes**

This subsection discusses the fabrication processes used in the case of bionanocomposites reinforced with agro-industrial wastes.

### **18.4.1 Using tea waste**

#### **18.4.1.1 Preparation of tea waste**

The use of tea waste taken from various factories to remove lead and cadmium ions from water has been performed (Joshi, Kataria, Garg, & Kadirvelu, 2020). The waste tea leaves that were taken from factories were cleaned properly and then dried for 12 h at 80°C. They were then powdered filtered by a mesh of 1.40 mm mesh sieve. The powder was then further dried for 1 h at 100°C (Joshi et al., 2020).

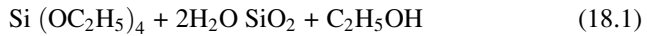
#### **18.4.1.2 Fabrication of silica nanoparticles**

The silica nanoparticles, fabricated by the modified Stober method described by Saini et al. (Saini, Garg, & Gupta, 2018, 2020), use a 2:1 ratio of absolute ethanol and water mix. The mix is kept in the ultrasonication bath for 15 min. Then 10 mL of liquid ammonia was dropwise added to the mix. After this reaction, 5 mL of tetraethoxysilane was added, which was then sonicated for 60 min. Doing so gives a white

color gel which was then centrifuged and washed with Millipore water. The resultant was kept in a hot air oven for 5 h at 70°C, which gives us the silica nanoparticles; the nanoparticles were then stored in plastic bottles (Saini et al., 2018, 2020).

### 18.4.1.3 Synthesis of bionanocomposite

Then 1.5 g waste tea leaves powder was added to Millipore water and stirred for 10 min without interruption. To this solution, stirring at room temperature for 30 min dispersed 3.0 g of silica nanoparticles. This suspension was sonicated for 60 min. The substance evolved was then centrifuged. Then it was washed and dried at 80°C for 3 h in a hot air oven. This resulting ash substance produced was SiO<sub>2</sub>-tea waste (TW) bionanocomposite. The experiment was materialized by the two following Eqs. (18.1) and (18.2):



This equation describes the synthesis of silica nanoparticles. The second equation is



This equation shows the residual tea waste being loaded by the silica nanoparticles (Joshi et al., 2020).

## 18.4.2 Using waste jackfruit peels

### 18.4.2.1 Preparation of plant material

Jackfruit peels were used to isolate pectin (Govindaraj, Rajan, Hatamleh, & Munusamy, 2018). For this procedure, the peels of jackfruit were removed after washing in double-distilled water, and then flushed with 250 mL dimethyl ketone. After being slashed into fine pieces, they were dried at 50°C for 24 h. When dried, they were ground and then refrigerated (Govindaraj et al., 2018).

### 18.4.2.2 Pectin isolation from jackfruit peel

The cell wall material (CWM) was removed from the ground peels using a 1:2 toluene to ethanol for 10 h and was separated using a vacuum pump. The particles were finely washed with 70% aqueous ethyl alcohol for the removal of pigment, dirt, and sugars until found colorless. The solvent was then changed to ethyl alcohol and dimethyl ketone and then dehydrated inside an oven at 50°C for 24 h (Govindaraj et al., 2018).

### 18.4.2.3 Partial isolation of pectin from the cell wall material

The dehydrated cell wall material was mixed in double-distilled water and sonicated at 50°C for 60 min, after which the residue is allowed to cool. The material is then separated through centrifugation at 6000 rpm and then it is filtered through Whatmann

no.1 filter paper. In double-distilled water, the residue is suspended and this mix is then combined with second isolation. After this process is completed, it is again centrifuged and then treatment with four volumes of ethyl alcohol is done to isolate and contain the hydrophilic pectin. This substance was dried and filtered at 50°C for utilization (Govindaraj et al., 2018).

#### **18.4.2.4 Synthesis of bionanocomposites**

To fabricate the nanocomposite, the jackfruit peel pectin was taken at 0.05 wt% and dissolved in double-distilled water, and sonicated at a frequency of 20 kHz for 60 min at 50°C. After sonication is done, 0.42 M CaCl<sub>2</sub>·4H<sub>2</sub>O is added to this solution. Following this, the pectin polymer solution was sonicated for 10 min. When this procedure is done, the pH was adjusted to 9.0 by NaOH. To this solution, 0.25 M K<sub>2</sub>HPO<sub>4</sub> was added and sonicated, which gives a white precipitate. Using warm air this suspension was dehydrated in a warm air oven and then was rinsed with double-distilled water and ethyl alcohol for the generation of bionanocomposites particles (Govindaraj et al., 2018).

### **18.4.3 Using waste turmeric spent**

#### **18.4.3.1 Isolation of dietary fiber (DF) from turmeric residue**

To first isolate the dietary fiber (DF) from the turmeric residue, the turmeric spent were cleaned first under running water then with the help of Millipore water, and dried later. The cleaned turmeric residue was washed with 1.7 wt% of liquid sodium chlorite in water for 2 h at 90°C. The pH was kept at 4 for the enhancement of bleaching action. The obtained fiber was then washed with distilled water for the attainment of a neutral pH, which was then further dried at 50°C for 12 h in an airflow oven (Gopi, Amalraj, Jude, Thomas, & Guo, 2019).

#### **18.4.3.2 Turmeric nanofiber preparation**

The DF isolated from the turmeric residue was used to prepare the turmeric nanofiber (Gopi et al., 2017; Kanimozhi, Basha, Kumari, Kaviyarasu, & Maaza, 2018). The TDF was grounded in a mixer and treated with alkali at 4% NaOH solution for 2 h at 80°C under a mechanical stirrer for the solubilization of lignin, hemicelluloses, and pectin. This process is repeated three times to remove the above-mentioned substances to ease the purification of cellulose. The fibers were continuously washed with the aid of distilled water to entirely remove the alkali after each treatment and were frequently checked for pH. The fibers were bleached using 1.7% (w/w) aqueous sodium chlorite in water, distilled water, and acetate buffer. This was again done thrice with the aid of a mechanical stirrer. This process was conducted to remove any traces of color. The validation of removal of phenolic compounds and lignin was performed after every bleaching session (Gopi et al., 2019). The next step in the procedure was acid hydrolysis by exposing about 6%–8% (w/w) of the bleached fiber at 50°C added to 65% (w/w) sulfuric acid for 1 h using a mechanical stirrer. This acid hydrolysis

facilitates the removal of traces of minerals, starch, and hydrolyzed amorphous cellulose. To terminate the reaction, ice cubes are added which also dilute the suspension. Then the fibers were properly cleaned with distilled water and then centrifuged at 10,000rpm at 10°C for 20 min. The NF was then homogenized using homomixer and then this step is repeated three times for 10 min each and then filtered using a glass filter (Gopi et al., 2019).

### **18.4.3.3 Synthesis of bionanocomposites**

Finally, the bionanocomposites were fabricated using the solvent casting technique, taking care of suitable adaptations as described by Pelissari et al. (Pelissari et al., 2017). The calculated weight of TNF was taken in 100 mL distilled water and stirred in a stirrer for 30 min. Afterward, it is sonicated in an ultrasonic bath sonicator for 15 min. Similarly, preweighed PS/TS/CS was stirred in 100 mL for 15 min in a mechanical stirrer. Then while being stirred for 30 min, TNF suspension was added to the water solution of PS/TS/CS. This suspension was further stirred for 30 min to homogenize and then heated to 80°C. During heating, this temperature was kept for 15 min and glycerol of 25 wt% of starch, was added to it. When the solution turned viscous, it was sonicated for 10 min. The solution is then transferred onto acrylic plates at 60°C to retain constant thickness. Another film called control film, which did not contain TNF, was prepared to check the total accumulation of TNF. The suspended films of potato starch-turmeric nanofiber (PS-TNF), tapioca starch-turmeric nanofiber (TS-TNF), and chitosan-turmeric nanofiber (CS-TNF) composites were created at 1%, 3%, 5%, and 7% of TNF concentration (as per dry wt PS/TS/CS) (Kanimozhi et al., 2018; Kanimozhi, Basha, & Kumari, 2016; Pelissari et al., 2017). The nanocomposites films were kept in relative humidity of 50% at about 25°C (Gopi et al., 2019).

## **18.4.4 Using spent hens**

### **18.4.4.1 Microwave-assisted lipid extraction**

To obtain the lipids, whole ground spent hens underwent microwave-assisted lipid extraction, for 10 min at 80°C (Safder, Temelli, & Ullah, 2019).

### **18.4.4.2 Synthesis of monomer and polymer**

In 24.7 g of oil, 230 mL of dichloromethane (DCM) and 23 mL methanol were dissolved. Further to this mix, 112 mL of 2N KOH solution in MeOH was added in a 500 mL flask and was then stirred for 2 h at 35°C. To confirm completion of this reaction, they were tested by thin-layer chromatography (TLC) and proton nuclear magnetic resonance spectroscopy (<sup>1</sup>HNMR) spectroscopy. The organic phase was then completely removed using a separatory funnel, after which another 200 mL of DCM completely remove all nonpolar compounds. The pH was adjusted between 1 and 2 with the aid of concentrated HCl. After checking for the pH using litmus paper

and using DCM, the free fatty acids were extracted. This extraction is done thrice with 200 mL of DCM and using the rotary evaporator under vacuum, the DCM was separated (Safder, Temelli, & Ullah, 2020).

Using a method reported by Khanra et al. (Khanra et al., 2018), the spent hen-derived fatty acid monomer (SFAM) was prepared. To elaborate, 8 g of hydrolyzed free fatty acids and 0.353 g of dimethylaminopyridine were mixed with 30 mL DCM in a 250 mL flask. After stirring this mixture, the reaction mixture was purged for 10 min in nitrogen ( $N_2$ ) in an ice bath. Using a separate beaker, 6.43 g of dicyclohexylcarbodiimide (DCC) were dissolved in 10 mL of DCM. This mixture was added to the previous mixture reaction dropwise. Afterward, 3.13 mL of 2-hydroxyethylacrylate was slowly added dropwise for an approximate time of 30 min. After removing the ice bath after 20 min, this mix was stirred overnight at 25°C. Using TLC, the progress of reaction until the reactant was completely utilized. For the removal of white precipitate, the mixture was filtered and then was followed by 60 mL of distilled water addition in the filtrate. The organic layer in this mix is then washed using  $4 \times 80$  mL of a saturated solution  $NaHCO_3$  and  $2 \times 80$  mL of brine, and after this process is complete, it is dried using anhydrous  $Na_2SO_4$  for a time period of 18 h. Using a rotary evaporator, the solvent was removed and the monomer extracted was cleaned via column chromatography with the help of silica and a 95:5 v/v mix of hexane and ethyl acetate, respectively, as the mobile phase (Khanra et al., 2018).

In 2016, Fortunati and team gave the equations for yield of the lipid hydrolysis and the yield of monomer extracted (Fortunati et al., 2016):

For the synthesis of spent hen-derived fatty acid polymer (SFAP), 1.5 g of SFAM were put into a flask of 25 mL together in a magnetic stirrer. Using a parafilm with a septum, the top was sealed. The mixture is kept in nitrogen for 15 min and then 20 mg of azobisisobutyronitrile (AIBN) initiator was mixed when a temperature of 70°C was attained. After this was done the reaction was allowed to ensue for 24 h. Temperatures of 70°C, 90°C, 110°C and reaction times of 2, 4, 8, 12, 15, and 24 h were tested for the optimization of the reaction and to get a high molecular weight polymer (Safder et al., 2020).

#### 18.4.4.3 *In situ dispersion of nanoclay and synthesis of nanocomposite*

For the in situ nanoclay dispersion and the synthesis of the nanocomposite, 1.5 g of SFAM and three different weight percentages, i.e., 3%, 5%, and 10% by weight of modified nanoclay were placed in a flask and the temperature was increased to 50°C for the liquefaction of mixture components. The mixtures are then stirred for 10 min followed by another 10 min of sonication to completely disperse nanoclay in the reaction mixture. This procedure is repeated thrice to ensure complete dispersion. To remove the air entrapped in the mix, the mix is purged with nitrogen. Then 20 mg AIBN initiator is added and the temperature is increased up to 70°C for the initiating polymerization. To remove any unreacted monomer, tetrahydrofuran was used (Safder et al., 2020).

#### 18.4.4.4 *Synthesis of bionanocomposite*

To fabricate the bionanocomposites, the films were prepared by compression molding. The films were exposed to a carver press, at a temperature of 150°C for 10 min, and a pressure of 3.45–4.83 MPa was applied. The films were then cut into a dimension of 30 mm in length, 10 mm of width, and 1 mm in thickness for further testing (Safder et al., 2020).

### 18.4.5 *Using waste sunflower stalk*

#### 18.4.5.1 *Extraction of cellulose nanocrystals*

To start the fabrication, we first extract cellulose in the form of nanocrystals. To do so, sunflower stalks have to be chemically pretreated. Several times, the stalks were washed with water, and then manually, the internal white pit was removed. First, the external fibrous structure was treated to 5% (wt/v) NaOH solution at room temperature (around 25°C) for 3 days where the liquid to fiber ratio is about 30:1, then it is treated with 5% (wt/v) NaOH solution for 2 h at 98°C where the liquid to fiber ratio is about 10:1. Furthermore, the structure was then treated with 5% (wt/v) of sodium chlorite where the bleaching fiber to liquid ratio was about 1:50, which was kept at pH = 4 and boiled for 2 h. After this bleaching process, it was treated to 5% (wt/v) of sodium bisulfate solution at room temperature for 30 min. A final treatment with 17.5% (wt/v) NaOH solution was done at room temperature for 20 min (Fortunati et al., 2016).

Sulfuric acid hydrolysis was done to create cellulose nanocrystals (CNC) water suspensions with the help of pretreated fibers (Bernhart & Fasina, 2009; Hong, Roy, Chalamaiyah, Bruce, & Wu, 2018). In brief, for hydrolysis 64% (wt/v) of sulfuric acid was taken and the suspensions were treated for 45°C for 30 min. After hydrolysis was complete, to remove excess acid, a centrifugation process at 4400 rpm for 20 min and a dialysis procedure of about 5–7 days was done. For the adjustment of negative charges induced by the preceding hydrolysis, a mixed bed ion exchange resin was added to the corresponding cellulose suspension for 48 h and then removed by filtration. The obtained cellulose nanocrystal aqueous suspension was ultrasonicated using a tip sonicator for 5 min. The resultant CNC water suspension was about 0.5% (wt/wt). The final yield when the hydrolysis was done was % of the initial weight of the pretreated sunflower fibers (Safder et al., 2020).

#### 18.4.5.2 *Extraction of cellulose nanofibrils*

Then, to extract the cellulose nanofibrils (CNF), steam explosion treatment was done. When comparing with alternative pretreatment methods present in the industry, steam explosion presents many advantages including lower capital investment, less hazardous process chemicals, and an exponentially lower environmental impact. The process involved first an alkali treatment with the steam explosion and then a bleaching and mild hydrolysis along with steam explosion. Cutting up the stalks into tiny pieces with a grinder, 100 g of them were taken and treated with 5% wt NaOH solution and were then kept in a laboratory autoclave, model no: KAUC-A1, which can operate at

137 Pa, for the steam explosion treatment. The temperature kept was 180°C for 1.5 h. Then to bleach, the resultant stalk sample treated with alkali, 5% wt sodium hypochlorite solution was used. This was done six times until the residue became white-colored. When bleaching was complete, the resultant white-colored fiber was washed, dried, and then subjected to mild acid hydrolysis with the help of 5% oxalic acid under the pressure of 137 Pa of the autoclave for 20 min. This process was also repeated six times. The fibers were again washed dried and thoroughly dispersed in water and properly homogenized while being continuously stirred for 6 h. The resultant obtained was cellulose nanofiber aqueous suspension. Using deionized water, the product was centrifuged to neutralization (Luzi et al., 2014).

### 18.4.5.3 Synthesis of bionanocomposites

Finally, to fabricate the nanocomposite using wheat gluten using CNC and CNF, 1% wt and 3% wt w.r.t. the matrix weight of CNC of density  $1.3 \text{ g cm}^{-3}$  and CNF of density  $1.5 \text{ g cm}^{-3}$  (Tuli et al., 2020) were taken. In brief, the fabrications were named Gluten\_1CNC, Gluten\_3CNC, Gluten\_1CNF, and Gluten\_3CNF. The volume fractions of CNC and CNF w.r.t. the gluten volume used is 0.47% (v/v), 1.45% (v/v), 0.41% (v/v), and 1.26% (v/v), respectively. As a plasticizer, deionized water mixed with 2% wt glycerol was utilized. Wheat gluten that was dispersed in 10% wt in the prepared solution with magnetic stirring at a high speed. Then sodium hydroxide solution at 0.5 M was added into the solution using magnetic stirring at room temperature at 30°C at a low speed until the pH of 10.8 was recorded. A following heated water bath, at 70°C for 10 min was applied under controlled pH. After cooling was done, both CNC and CNF aqueous dispersions were mixed and stirred magnetically for 30 min at room temperature. For casting, they were cast on Teflon sheets, and drying was done at room temperature. When the films were removable, they formed sheets that were 90–100  $\mu\text{m}$  thick were obtained. The films were then conditioned at 20°C and relative humidity of 53% in the desiccator, with the aid of magnesium nitrate-6-hydrate saturated solution for a weak. Gluten-based films were produced using the exact procedure and the excessive use of water was also kept under consideration (Jonoobi, Harun, Mathew, & Oksman, 2010).

## 18.5 Physical properties and tribology of different bionanocomposite reinforced by agro-industrial wastes

### 18.5.1 Sugar palm fiber

Sugar palm fiber is one of the bionanocomposites reinforced by agro-industrial waste and is also known as Ijuk (black/brown in color) (Rashid, Leman, Jawaid, Ghazali, & Ishak, 2016). It possesses a density ( $\text{g/cm}^3$ ) of 1.21 (if having a diameter ( $\mu\text{m}$ ) of 81–500 ( $\mu\text{m}$ )). Then it has got the high strength that is tensile strength of 276 MPa, tensile modulus of 3.847 GPa and elongation at break is 12.8%. It is quite good

biodegradable with crystallinity of 55.8% (Razak & Ferdiansyah, 2005; Sanyang, Sapuan, Jawaid, Ishak, & Sahari, 2016). It has lower durability than synthetic fiber and is also quite easily available, and is of low in cost (Ilyas, Sapuan, Ishak, & Zainudin, 2017).

### **18.5.2 Sisal**

Sisal fiber is one of the natural fibers, which are found from sisal green leaf. It has a density ( $\text{g/cm}^3$ ) of 1.33–1.5 (if it has the diameter ( $\mu\text{m}$ ) of 50–300) (Chand & Fahim, 2008; Sreekumar et al., 2009). Then it has got the strength that is tensile strength of 511–635 MPa, tensile modulus of 9.4–22 GPa, and elongation at break is 2%–2.5%. It is quite a good natural biodegradable matter (de Andrade Silva, Toledo Filho, de Almeida Melo Filho, & Fairbairn, 2010).

### **18.5.3 Coir**

Coir is a versatile natural fiber extracted from mesocarp tissue, or husk of the coconut fruit. Generally, fiber is of golden color when cleaned after removing from coconut husk; and hence the name “The Golden Fiber.” It possesses a density of 1.2 ( $\text{g/cm}^3$ ) (If having a diameter of 100–450  $\mu\text{m}$ ). It has a high tensile strength of 248 MPa, tensile modulus of 4.94 GPa, and elongation at break is 30% (Ayrilmis, Jarusombuti, Fueangvivat, Bauchongkol, & White, 2011; Defoirdt et al., 2010; Fouladi, Ayub, & Nor, 2011).

### **18.5.4 Ramie fiber**

Ramie is one of the strongest natural fibers. It exhibits even greater strength when wet. Ramie fiber is known especially for its ability to hold shape, reduce wrinkling, and introduce a silky luster to the fabric appearance. It is not as durable as other fibers, and so is usually used as a blend with other fibers such as cotton or wool (Chakravarty, Sen, & Dasgupta, 1991). It has the density of 1.5  $\text{g/cm}^3$ . If having a diameter of 46–53.2  $\mu\text{m}$ , then it has got the high strength that is tensile strength of 400–938 MPa, tensile modulus of 61.4–128 GPa, and elongation at break is 3.6%–3.8% (Syafri, Kasim, Abral, & Asben, 2018).

### **18.5.5 Hemp**

Hemp, or industrial hemp, is a variety of the *Cannabis sativa* plant species that is grown specifically for industrial use. It can be used to make a wide range of products (Mwaikambo & Ansell, 2006). It has the density of 1.47  $\text{g/cm}^3$ . If having a diameter of 17–23  $\mu\text{m}$ , then it has got the high strength that is tensile strength of 690 MPa, tensile modulus of 70 GPa, and elongation at break is 2%–4% (Dhakal, Zhang, & Richardson, 2007).



### **18.5.6 Flax**

Flax fiber is obtained from the inner bark of the stem of a plant grown in temperate and subtropical regions of the world. It is a natural, cellulosic, and multicellular bast fiber. Flax fiber has the density of 1.4–1.5 g/cm<sup>3</sup>. If having a diameter of 11.3–23 μm, then it has got the high strength that is tensile strength of 1339 MPa, tensile modulus of 54.08 GPa, and elongation at break is 3.27% (Kalia et al., 2011; Sharma, Faughey, & Lyons, 1999).

### **18.5.7 Kenaf (bast)**

Kenaf fiber has emerged as an important plant cultivated in third-world countries and has been regarded as an industrial crop. It has a great potential for replacing synthetic fiber such as glass fiber. The use of kenaf fiber can provide mechanical properties, i.e., tensile strength, comparable to those of synthetic fiber with lower density than traditional materials, resulting in lightweight and eco-friendly polymer composites. It has a density of 1.45 g/cm<sup>3</sup>. If having a diameter of 70–250 μm, then it has got the high strength that is tensile strength of 295 MPa, tensile modulus of 53 GPa, and elongation at break is 1.6% (Hashim et al., 2017; Jonoobi, Harun, Mishra, & Oksman, 2009).

### **18.5.8 Sugarcane bagasse**

Sugarcane bagasse ash (SCBA) is an abundant by-product of the sugar and ethanol industry. SCBA is generally used as a fertilizer or is disposed of in landfills, which has led to intensified environmental concerns (Xu, Ji, Gao, Yang, & Wu, 2019). Dark black indicates higher carbon content, mainly due to incomplete combustion. Owing to crystallization and decomposition at high temperatures, SCBA appears gray above 800°C recalcination temperature and appears white above 900°C, and has got the crystallinity of 76% (De et al., 2011; Loh, Sujun, Rahman, & Das, 2013).

### **18.5.9 Wheat straw fiber**

Wheat straw is the stalk left over after wheat grains are harvested. Traditionally, it has been treated as a waste. In some countries, farmers burn it, contributing to air pollution and creating a public health hazard. However, these stalks still have value. We reclaim this material and use it to make our wheat straw products. Wheat straw is very versatile and can be used for many different products. Since plastic made from wheat straw is very durable and heat-resistant, it can resist temperatures up to 200°F. It's a great material to make mugs and cups (Alemdar & Sain, 2008; Pan, Zhou, Deng, & Zhang, 2009). The physical appearance of the wheat straw is dense and smooth. It is also porous and has lower epidermis. It shows the highest tensile strength when treated with 2% of NaOH that is 287 MPa. It also shows the highest tensile modulus when treated with 2% of NaOH that is 10.2 GPa, and the crystallinity of the wheat straw fiber is 57.5% (Yang, He, Liu, & Diao, 2016).

### **18.5.10 Soy hull fiber**

Soybean straw is a lignocellulosic agricultural stalk. It's plentiful, inexpensive, and renewable. But most of the soybean straw is arbitrarily discarded or set on fire. It consists of 38% cellulose, 16% hemicelluloses, 16% lignin, 0.83% nitrogen, and 6% ash (Cardoso, Oliveira, Junior, & Ataíde, 2013). The soybean straw that was washed (with water or base (0.1 M NaOH)) and CA modified to enhance its natural adsorption capacity. And the crystallinity (i.e., in %) of the wheat straw fiber is 59.8% (Alemdar & Sain, 2008).

### **18.5.11 Banana fiber**

Banana fiber, also known as musa fiber, is one of the world's strongest natural fibers. This natural fiber is made from the stem of the banana tree and is incredibly durable. The fiber consists of thick-walled cell tissue, bonded together by natural gums and is mainly composed of cellulose, hemicelluloses, and lignin. Banana fiber is similar to natural bamboo fiber, but its spin ability, fineness, and tensile strength are said to be better. Banana fiber can be used to make a number of different textiles with different weights and thicknesses, based on what part of the banana stem the fiber was extracted from. The thicker, sturdier fibers are taken from the banana trees outer sheaths, whereas the inner sheaths result in softer fibers (Senthilkumar, Siva, Rajini, Jappes, & Siengchin, 2018). Banana fiber has got the density of 1.350 g/cc. The tensile strength of the banana fiber is  $550 \pm 6.8$  MPa, and the Young's modulus (in GPa) of the banana fiber is 3.5 GPa. The cellulose present is 63%–64% in banana fiber. The moisture content present is 10%–11%, and rest hemicellulose and lignin are 19% and 5%, respectively. The crystallinity content present in it is 25% (Tibolla, Pelissari, & Menegalli, 2014).

### **18.5.12 Coconut sheath**

Coconut leaf sheath fibers occur in mat form. The leaf sheaths collected from the trees are thoroughly washed with tap water followed by distilled water. Mostly, coconut sheath fiber has been used to prepare the composite material with epoxy resin. First the untreated coconut fiber was used to prepare the composite material then the coconut sheath fibers were treated with NAOH to modify the fiber properties (Jappes, Siva, & Rajini, 2012; Santhanam & Kumaravel, 2014). The cellulose (%) present in it is 68%, and the hemicellulose (%) and lignin (%) contents present in the coconut sheath are 22% and 20.6%, respectively. The density of the coconut sheath is 1.375 g/cc. The physical property the tensile strength is 88.63 MPa, and the Young's modulus is 4.4 GPa (Kumar, Siva, Rajini, Jappes, & Amico, 2016). In addition, the authors have a vast experience in this field of bio- and nanocomposites (Arpitha, Verma, Sanjay, & Siengchin, 2021; Bharath et al., 2020; Bisht, Verma, Chauhan, & Singh, 2021; Chaudhary, Sharma, & Verma, 2022a, 2022b; Chaurasia, Verma, Parashar, & Mulik, 2019; Deji, Verma, Choudhary, & Sharma, 2021; Deji, Verma, Kaur, Choudhary, & Sharma, 2022; Jain, Verma, & Singh, 2019; Kataria,

Verma, Sanjay, & Siengchin, 2022; Rastogi, Verma, & Singh, 2020; Singh, Jain, Verma, Singh, & Chauhan, 2020; Singla, Verma, & Parashar, 2018; Verma, Jain, Kalpana, et al., 2020; Verma, Jain, Rastogi, et al., 2020; Verma, Parashar, Singh, et al., 2020; Verma, Parashar, Jain, et al., 2020; Verma et al., 2020a, 2020b; Verma, Jain, Parashar, et al., 2021; Verma, Baurai, Sanjay, & Siengchin, 2020; Verma, Budiya, Sanjay, & Siengchin, 2019; Verma, Gaur, & Singh, 2017; Verma, Joshi, Gaur, & Singh, 2018; Verma, Kumar, & Parashar, 2019; Verma, Negi, & Singh, 2018a, 2018b, 2019; Verma & Parashar, 2017, 2018a, 2018b, 2018c, 2020; Verma, Parashar, & Packirisamy, 2018a, 2018b, 2019a, 2019b; Verma & Singh, 2016, 2019; Verma, Singh, & Arif, 2016; Verma, Singh, Singh, & Jain, 2019; Verma, Singh, Verma, & Sharma, 2016; Verma, Zhang, & Van Duin, 2021).

## Acknowledgment

Monetary and academic support from the University of Petroleum and Energy Studies, Dehradun, India (SEED Grant program) is highly appreciable.

## Conflicts of interest

There are no conflicts of interest to declare by the authors.

## References

- Abdulkhani, A., Mazhar, A. N., Hedjazi, S., & Hamzeh, Y. (2019). Preparation of xylan bio-composite films reinforced with oxidized carboxymethyl cellulose and nanocellulose. *Polymer Bulletin*, 1–13.
- Alemdar, A., & Sain, M. (2008). Isolation and characterization of nanofibers from agricultural residues—wheat straw and soy hulls. *Bioresource Technology*, 99(6), 1664–1671.
- Almeida, V. S. D., Barretti, B. R. V., Ito, V. C., Malucelli, L., Carvalho Filho, M. A. D. S., Demiate, I. M., et al. (2020). Thermal, morphological, and mechanical properties of regular and waxy maize starch films reinforced with cellulose nanofibers (CNF). *Materials Research*, 23(2).
- Arpitha, G. R., Verma, A., Sanjay, M. R., & Siengchin, S. (2021). Preparation and experimental investigation on mechanical and tribological performance of hemp-glass fiber reinforced laminated composites for lightweight applications. *Advances in Civil Engineering Materials*, 10(1), 427–439.
- Ayirmis, N., Jarusombuti, S., Fueangvivat, V., Bauchongkol, P., & White, R. H. (2011). Coir fiber reinforced polypropylene composite panel for automotive interior applications. *Fibers and Polymers*, 12(7), 919–926.
- Bernhart, M., & Fasina, O. O. (2009). Moisture effect on the storage, handling and flow properties of poultry litter. *Waste Management*, 29(4), 1392–1398.
- Bharath, K. N., Madhu, P., Gowda, T. G., Verma, A., Sanjay, M. R., & Siengchin, S. (2020). A novel approach for development of printed circuit board from biofiber based composites. *Polymer Composites*, 41(11), 4550–4558.
- Bisht, N., Verma, A., Chauhan, S., & Singh, V. K. (2021). Effect of functionalized silicon carbide nano-particles as additive in cross-linked PVA based composites for vibration damping application. *Journal of Vinyl and Additive Technology*, 27(4), 920–932.

- Cardoso, C. R., Oliveira, T. J. P., Junior, J. S., & Ataíde, C. H. (2013). Physical characterization of sweet sorghum bagasse, tobacco residue, soy hull and fiber sorghum bagasse particles: Density, particle size and shape distributions. *Powder Technology*, 245, 105–114.
- Chakravarty, A. C., Sen, S. K., & Dasgupta, P. C. (1991). Studies on ramie fiber, the effect of gum content on the physical properties of ramie fiber. *Journal of Textile Association*, 33, 73.
- Chand, N., & Fahim, M. (2008). *Woodhead publishing series in composites science and engineering, tribology of natural fiber polymer composites*. Woodhead Publishing. <https://doi.org/10.1533/9781845695057.84>.
- Chaudhary, A., Sharma, S., & Verma, A. (2022a). WEDM machining of heat treated ASSAB'88 tool steel: A comprehensive experimental analysis. *Materials Today: Proceedings*, 50(Part 5), 946–951.
- Chaudhary, A., Sharma, S., & Verma, A. (2022b). Optimization of WEDM process parameters for machining of heat treated ASSAB'88 tool steel using response surface methodology (RSM). *Materials Today: Proceedings*, 50(Part 5), 917–922.
- Chaurasia, A., Verma, A., Parashar, A., & Mulik, R. S. (2019). Experimental and computational studies to analyze the effect of h-BN nanosheets on mechanical behavior of h-BN/polyethylene nanocomposites. *The Journal of Physical Chemistry C*, 123(32), 20059–20070.
- Chen, C., Wang, H., Li, S., Fang, L., & Li, D. (2017). Reinforcement of cellulose nanofibers in polyacrylamide gels. *Cellulose*, 24(12), 5487–5493.
- de Andrade Silva, F., Toledo Filho, R. D., de Almeida Melo Filho, J., & Fairbairn, E. D. M. R. (2010). Physical and mechanical properties of durable sisal fiber–cement composites. *Construction and Building Materials*, 24(5), 777–785.
- De, M. E., Jessika, T., Bruna, K., Teodoro, R., Carolina, A., Manoel, J., et al. (2011). Sugarcane bagasse whiskers: Extraction and characterizations. *Industrial Crops and Products*, 33, 66. <https://doi.org/10.1016/j.indcrop.2010.08.009>.
- Defoirdt, N., Biswas, S., De Vriese, L., Van Acker, J., Ahsan, Q., Gorbatikh, L., et al. (2010). Assessment of the tensile properties of coir, bamboo and jute fibre. *Composites Part A: Applied Science and Manufacturing*, 41(5), 588–595.
- Deji, R., Verma, A., Choudhary, B. C., & Sharma, R. K. (2021). New insights into NO adsorption on alkali metal and transition metal doped graphene nanoribbon surface: A DFT approach. *Journal of Molecular Graphics and Modelling*, 111, 108109.
- Deji, R., Verma, A., Kaur, N., Choudhary, B. C., & Sharma, R. K. (2022). Density functional theory study of carbon monoxide adsorption on transition metal doped armchair graphene nanoribbon. *Materials Today: Proceedings*, 54(Part 3), 771–776.
- Dhakal, H. N., Zhang, Z. A., & Richardson, M. O. W. (2007). Effect of water absorption on the mechanical properties of hemp fibre reinforced unsaturated polyester composites. *Composites Science and Technology*, 67(7–8), 1674–1683.
- Fortunati, E., Luzzi, F., Jiménez, A., Gopakumar, D. A., Puglia, D., Thomas, S., et al. (2016). Revalorization of sunflower stalks as novel sources of cellulose nanofibrils and nanocrystals and their effect on wheat gluten bionanocomposite properties. *Carbohydrate Polymers*, 149, 357–368.
- Fouladi, M. H., Ayub, M., & Nor, M. J. M. (2011). Analysis of coir fiber acoustical characteristics. *Applied Acoustics*, 72(1), 35–42.
- Ghadikolaei, S. S., Omrani, A., & Ehsani, M. (2018). Influences of modified bacterial cellulose nanofibers (BCNs) on structural, thermophysical, optical, and barrier properties of poly ethylene-co-vinyl acetate (EVA) nanocomposite. *International Journal of Biological Macromolecules*, 115, 266–272.

- Ghanbari, A., Tabarsa, T., Ashori, A., Shakeri, A., & Mashkour, M. (2018). Thermoplastic starch foamed composites reinforced with cellulose nanofibers: Thermal and mechanical properties. *Carbohydrate Polymers*, *197*, 305–311.
- Gopi, S., Amalraj, A., Jude, S., Thomas, S., & Guo, Q. (2019). Bionanocomposite films based on potato, tapioca starch and chitosan reinforced with cellulose nanofiber isolated from turmeric spent. *Journal of the Taiwan Institute of Chemical Engineers*, *96*, 664–671.
- Gopi, S., Amalraj, A., Jude, S., Varma, K., Sreeraj, T. R., Haponiuk, J. T., et al. (2017). Preparation, characterization and anti-colitis activity of curcumin-asafetida complex encapsulated in turmeric nanofiber. *Materials Science and Engineering: C*, *81*, 20–31.
- Govindaraj, D., Rajan, M., Hatamleh, A. A., & Munusamy, M. A. (2018). From waste to high-value product: Jackfruit peel derived pectin/apatite bionanocomposites for bone healing applications. *International Journal of Biological Macromolecules*, *106*, 293–301.
- Guleria, A., Singha, A. S., & Rana, R. K. (2017). Preparation of starch-based biocomposites reinforced with mercerized lignocellulosic fibers: Evaluation of their thermal, morphological, mechanical, and biodegradable properties. *International Journal of Polymer Analysis and Characterization*, *22*(7), 595–609.
- Hashim, M. Y., Amin, A. M., Marwah, O. M. F., Othman, M. H., Yunus, M. R. M., & Huat, N. C. (2017, October). The effect of alkali treatment under various conditions on physical properties of kenaf fiber. *Journal of Physics: Conference Series*, *914*(1), 012030.
- Hong, H., Roy, B. C., Chalamaiah, M., Bruce, H. L., & Wu, J. (2018). Pretreatment with formic acid enhances the production of small peptides from highly cross-linked collagen of spent hens. *Food Chemistry*, *258*, 174–180.
- Ilyas, R. A., Sapuan, S. M., Ishak, M. R., & Zainudin, E. S. (2017). Effect of delignification on the physical, thermal, chemical, and structural properties of sugar palm fibre. *BioResources*, *12*(4), 8734–8754.
- Ivdre, A., Mucci, V., Stefani, P. M., Aranguren, M. I., & Cabulis, U. (2016). Nanocellulose reinforced polyurethane obtained from hydroxylated soybean oil. *IOP Conference Series: Materials Science and Engineering*, *111*(1), 012011.
- Jain, N., Verma, A., & Singh, V. K. (2019). Dynamic mechanical analysis and creep-recovery behaviour of polyvinyl alcohol based cross-linked biocomposite reinforced with basalt fiber. *Materials Research Express*, *6*(10), 105373.
- Jappes, J. W., Siva, I., & Rajini, N. (2012). Fractography analysis of naturally woven coconut sheath reinforced polyester composite: A novel reinforcement. *Polymer-Plastics Technology and Engineering*, *51*(4), 419–424.
- Jonoobi, M., Harun, J., Mathew, A. P., & Oksman, K. (2010). Mechanical properties of cellulose nanofiber (CNF) reinforced polylactic acid (PLA) prepared by twin screw extrusion. *Composites Science and Technology*, *70*(12), 1742–1747.
- Jonoobi, M., Harun, J., Mishra, M., & Oksman, K. (2009). Chemical composition, crystallinity and thermal degradation of bleached and unbleached kenaf bast (*Hibiscus cannabinus*) pulp and nanofiber. *BioResources*, *4*(2), 626–639.
- Joshi, S., Kataria, N., Garg, V. K., & Kadirvelu, K. (2020). Pb<sup>2+</sup> and Cd<sup>2+</sup> recovery from water using residual tea waste and SiO<sub>2</sub>@ TW nanocomposites. *Chemosphere*, *257*, 127277.
- Joy, J., Jose, C., Varanasi, S. B., Lovely Mathew, P., Thomas, S., & Pilla, S. (2016). Preparation and characterization of poly (butylene succinate) bionanocomposites reinforced with cellulose nanofiber extracted from *Helicteres isora* plant. *Journal of Renewable Materials*, *4* (5), 351–364.
- Kalia, S., Dufresne, A., Cherian, B. M., Kaith, B. S., Avérous, L., Njuguna, J., et al. (2011). Cellulose-based bio- and nanocomposites: A review. *International Journal of Polymer Science*, *2011*, 837875.

- Kanimozhi, K., Basha, S. K., & Kumari, V. S. (2016). Fabrication of chitosan based hybrid porous scaffolds by salt leaching for soft tissue engineering. *Surfaces and Interfaces*, 1, 7–12.
- Kanimozhi, K., Basha, S. K., Kumari, V. S., Kaviyarasu, K., & Maaza, M. (2018). In vitro cytocompatibility of chitosan/PVA/methylcellulose–Nanocellulose nanocomposites scaffolds using L929 fibroblast cells. *Applied Surface Science*, 449, 574–583.
- Kataria, A., Verma, A., Sanjay, M. R., & Siengchin, S. (2022). Molecular modeling of 2D graphene grain boundaries: Mechanical and fracture aspects. *Materials Today: Proceedings*, 52(Part 5), 2404–2408.
- Khanra, S., Mondal, M., Halder, G., Tiwari, O. N., Gayen, K., & Bhowmick, T. K. (2018). Downstream processing of microalgae for pigments, protein and carbohydrate in industrial application: A review. *Food and Bioproducts Processing*, 110, 60–84.
- Kumagai, A., Tajima, N., Iwamoto, S., Morimoto, T., Nagatani, A., Okazaki, T., et al. (2019). Properties of natural rubber reinforced with cellulose nanofibers based on fiber diameter distribution as estimated by differential centrifugal sedimentation. *International Journal of Biological Macromolecules*, 121, 989–995.
- Kumar, K. S., Siva, I., Rajini, N., Jappes, J. W., & Amico, S. C. (2016). Layering pattern effects on vibrational behavior of coconut sheath/banana fiber hybrid composites. *Materials & Design*, 90, 795–803.
- Kurita, H., Ishigami, R., Wu, C., & Narita, F. (2021). Mechanical properties of mechanically-defibrated cellulose nanofiber reinforced epoxy resin matrix composites. *Journal of Composite Materials*, 55(4), 455–464.
- Loh, Y. R., Sujan, D., Rahman, M. E., & Das, C. A. (2013). Sugarcane bagasse—The future composite material: A literature review. *Resources, Conservation and Recycling*, 75, 14–22.
- Luz, S. M., Del Tio, J., Rocha, G. J. M., Gonçalves, A. R., & Del'Arco, A. P., Jr. (2008). Cellulose and cellulignin from sugarcane bagasse reinforced polypropylene composites: Effect of acetylation on mechanical and thermal properties. *Composites Part A: Applied Science and Manufacturing*, 39(9), 1362–1369.
- Luzi, F., Fortunati, E., Puglia, D., Lavorgna, M., Santulli, C., Kenny, J. M., et al. (2014). Optimized extraction of cellulose nanocrystals from pristine and carded hemp fibres. *Industrial Crops and Products*, 56, 175–186.
- Midhun Dominic, C. D., Joseph, R., Begum, P. M., Joseph, M., Padmanabhan, D., Morris, L. A., et al. (2020). Cellulose nanofibers isolated from the *Cuscuta Reflexa* plant as a green reinforcement of natural rubber. *Polymers*, 12(4), 814.
- Mulinari, D. R., Voorwald, H. J., Cioffi, M. O., & da Silva, M. L. (2017). Cellulose fiber-reinforced high-density polyethylene composites—Mechanical and thermal properties. *Journal of Composite Materials*, 51(13), 1807–1815.
- Mwaikambo, L. Y., & Ansell, M. P. (2006). Mechanical properties of alkali treated plant fibres and their potential as reinforcement materials. I. Hemp fibres. *Journal of Materials Science*, 41(8), 2483–2496.
- Neves, R. M., Lopes, K. S., Zimmermann, M. V. G., Poletto, M., & Zattera, A. J. (2019). Characterization of polystyrene nanocomposites and expanded nanocomposites reinforced with cellulose nanofibers and nanocrystals. *Cellulose*, 26(7), 4417–4429.
- Nissilä, T., Hietala, M., & Oksman, K. (2019). A method for preparing epoxy-cellulose nanofiber composites with an oriented structure. *Composites Part A: Applied Science and Manufacturing*, 125, 105515.
- Nuruddin, M., Gupta, R., Tcherbi-Narteh, A., Hosur, M., & Jeelani, S. (2015). Thermal and mechanical properties of cellulose nanofibers reinforced polyvinyl alcohol composite films. In *69th FPS international convention, Atlanta, GA*.

- Pan, M. Z., Zhou, D. G., Deng, J., & Zhang, S. Y. (2009). Preparation and properties of wheat straw fiber-polypropylene composites. I. Investigation of surface treatments on the wheat straw fiber. *Journal of Applied Polymer Science*, *114*(5), 3049–3056.
- Panaiteescu, D. M., Nicolae, C. A., Gabor, A. R., & Trusca, R. (2020). Thermal and mechanical properties of poly (3-hydroxybutyrate) reinforced with cellulose fibers from wood waste. *Industrial Crops and Products*, *145*, 112071.
- Pelissari, F. M., Andrade-Mahecha, M. M., do Amaral Sobral, P. J., & Menegalli, F. C. (2017). Nanocomposites based on banana starch reinforced with cellulose nanofibers isolated from banana peels. *Journal of Colloid and Interface Science*, *505*, 154–167.
- Ramezani Kakroodi, A., Cheng, S., Sain, M., & Asiri, A. (2014). Mechanical, thermal, and morphological properties of nanocomposites based on polyvinyl alcohol and cellulose nanofiber from *Aloe vera* rind. *Journal of Nanomaterials*, *2014*, 903498. <https://doi.org/10.1155/2014/903498>.
- Rani, A., Monga, S., Bansal, M., & Sharma, A. (2018). Bionanocomposites reinforced with cellulose nanofibers derived from sugarcane bagasse. *Polymer Composites*, *39*, E55–E64.
- Rashid, B., Leman, Z., Jawaid, M., Ghazali, M. J., & Ishak, M. R. (2016). Physicochemical and thermal properties of lignocellulosic fiber from sugar palm fibers: Effect of treatment. *Cellulose*, *23*(5), 2905–2916.
- Rastogi, S., Verma, A., & Singh, V. K. (2020). Experimental response of nonwoven waste cellulose fabric-reinforced epoxy composites for high toughness and coating applications. *Materials Performance and Characterization*, *9*(1), 151–172.
- Razak, H. A., & Ferdiansyah, T. (2005). Toughness characteristics of *Arenga pinnata* fibre concrete. *Journal of Natural Fibers*, *2*(2), 89–103.
- Saba, N., Mohammad, F., Pervaiz, M., Jawaid, M., Alothman, O. Y., & Sain, M. (2017). Mechanical, morphological and structural properties of cellulose nanofibers reinforced epoxy composites. *International Journal of Biological Macromolecules*, *97*, 190–200.
- Safdari, F., Carreau, P. J., Heuzey, M. C., & Kamal, M. R. (2017). Effects of poly (ethylene glycol) on the morphology and properties of biocomposites based on polylactide and cellulose nanofibers. *Cellulose*, *24*(7), 2877–2893.
- Safdari, F., Carreau, P. J., Heuzey, M. C., Kamal, M. R., & Sain, M. M. (2017). Enhanced properties of poly (ethylene oxide)/cellulose nanofiber biocomposites. *Cellulose*, *24*(2), 755–767.
- Safder, M., Temelli, F., & Ullah, A. (2019). Extraction, optimization, and characterization of lipids from spent hens: An unexploited sustainable bioresource. *Journal of Cleaner Production*, *206*, 622–630.
- Safder, M., Temelli, F., & Ullah, A. (2020). Lipid-derived hybrid bionanocomposites from spent hens. *Materials Today Communications*, *25*, 101327.
- Saini, J., Garg, V. K., & Gupta, R. K. (2018). Removal of methylene blue from aqueous solution by Fe<sub>3</sub>O<sub>4</sub>@ Ag/SiO<sub>2</sub> nanospheres: Synthesis, characterization and adsorption performance. *Journal of Molecular Liquids*, *250*, 413–422.
- Saini, J., Garg, V. K., & Gupta, R. K. (2020). Green synthesized SiO<sub>2</sub>@ OPW nanocomposites for enhanced Lead (II) removal from water. *Arabian Journal of Chemistry*, *13*(1), 2496–2507.
- Santhanam, K., & Kumaravel, A. (2014). Effect of fiber loading and surface treatment on the mechanical properties of coconut sheath fiber reinforced epoxy composites. *Advanced Materials Research*, *984*, 178–184.
- Sanyang, M. L., Sapuan, S. M., Jawaid, M., Ishak, M. R., & Sahari, J. (2016). Recent developments in sugar palm (*Arenga pinnata*) based biocomposites and their potential industrial applications: A review. *Renewable and Sustainable Energy Reviews*, *54*, 533–549.

- Senthilkumar, K., Siva, I., Rajini, N., Jappes, J. W., & Siengchin, S. (2018). Mechanical characteristics of tri-layer eco-friendly polymer composites for interior parts of aerospace application. In *Sustainable composites for aerospace applications* (pp. 35–53). Woodhead Publishing.
- Sharma, H. S. S., Faughey, G., & Lyons, G. (1999). Comparison of physical, chemical, and thermal characteristics of water-, dew-, and enzyme-retted flax fibers. *Journal of Applied Polymer Science*, 74(1), 139–143.
- Singh, K., Jain, N., Verma, A., Singh, V. K., & Chauhan, S. (2020). Functionalized graphite-reinforced cross-linked poly (vinyl alcohol) nanocomposites for vibration isolator application: Morphology, mechanical, and thermal assessment. *Materials Performance and Characterization*, 9(1), 215–230.
- Singla, V., Verma, A., & Parashar, A. (2018). A molecular dynamics based study to estimate the point defects formation energies in graphene containing STW defects. *Materials Research Express*, 6(1), 015606.
- Siva, R., Valarmathi, T. N., Venkatesh, S., Reddy, S. S., Pandurangan, P., & Karthikeyan, P. (2020). Mechanical characterization and microstructure analyses of nano cellulose fiber biodegradable composite. *Materials Today: Proceedings*.
- Sreekumar, P. A., Thomas, S. P., Saiter, J., Joseph, K., Unnikrishnan, G., & Thomas, S. (2009). Effect of fiber surface modification on the mechanical and water absorption characteristics of sisal/polyester composites fabricated by resin transfer molding. *Composites Part A: Applied Science and Manufacturing*, 40(11), 1777–1784.
- Syafri, E., Kasim, A., Abrial, H., & Asben, A. (2018). Cellulose nanofibers isolation and characterization from ramie using a chemical-ultrasonic treatment. *Journal of Natural Fibers*, 16(8), 1145–1155.
- Tibolla, H., Pelissari, F. M., & Menegalli, F. C. (2014). Cellulose nanofibers produced from banana peel by chemical and enzymatic treatment. *LWT- Food Science and Technology*, 59(2), 1311–1318.
- Tuli, F. J., Hossain, A., Kibria, A. F., Tareq, A. R. M., Mamun, S. M., & Ullah, A. A. (2020). Removal of methylene blue from water by low-cost activated carbon prepared from tea waste: A study of adsorption isotherm and kinetics. *Environmental Nanotechnology, Monitoring & Management*, 14, 100354.
- Verma, A., Baurai, K., Sanjay, M. R., & Siengchin, S. (2020). Mechanical, microstructural, and thermal characterization insights of pyrolyzed carbon black from waste tires reinforced epoxy nanocomposites for coating application. *Polymer Composites*, 41(1), 338–349.
- Verma, A., Budiya, L., Sanjay, M. R., & Siengchin, S. (2019). Processing and characterization analysis of pyrolyzed oil rubber (from waste tires)-epoxy polymer blend composite for lightweight structures and coatings applications. *Polymer Engineering & Science*, 59(10), 2041–2051.
- Verma, A., Gaur, A., & Singh, V. K. (2017). Mechanical properties and microstructure of starch and sisal fiber biocomposite modified with epoxy resin. *Materials Performance and Characterization*, 6(1), 500–520.
- Verma, A., Jain, N., Kalpana, Sanjay, M. R., Siengchin, S., & Jawaid, M. (2020). Natural fibers based bio-phenolic composites. In *Phenolic polymers based composite materials* (pp. 153–168). Singapore: Springer Nature (Chapter 10).
- Verma, A., Jain, N., Parashar, A., Gaur, A., Sanjay, M. R., & Siengchin, S. (2021). Lifecycle assessment of thermoplastic and thermosetting bamboo composites. In *Bamboo fiber composites* (pp. 235–246). Singapore: Springer.
- Verma, A., Jain, N., Parashar, A., Singh, V. K., Sanjay, M. R., & Siengchin, S. (2020a). Design and modeling of lightweight polymer composite structures. In *Lightweight polymer*



- composite structures: Design and manufacturing techniques* (pp. 193–224). Boca Raton: Taylor & Francis Group (CRC Press) (Chapter 7).
- Verma, A., Jain, N., Parashar, A., Singh, V. K., Sanjay, M. R., & Siengchin, S. (2020b). Light-weight graphene composite materials. In *Lightweight polymer composite structures: Design and manufacturing techniques* (pp. 1–20). Boca Raton: Taylor & Francis Group (CRC Press) (Chapter 1).
- Verma, A., Jain, N., Rangappa, S. M., Siengchin, S., & Jawaid, M. (2021). Natural fibers based bio-phenolic composites. In *Phenolic polymers based composite materials* (pp. 153–168). Singapore: Springer.
- Verma, A., Jain, N., Rastogi, S., Dogra, V., Sanjay, M. R., Siengchin, S., et al. (2020). Mechanism, anti-corrosion protection and components of anti-corrosion polymer coatings. In *Polymer coatings: Technologies and applications* (pp. 53–66). Boca Raton: Taylor & Francis Group (CRC Press) (Chapter 4).
- Verma, A., Joshi, K., Gaur, A., & Singh, V. K. (2018). Starch-jute fiber hybrid biocomposite modified with an epoxy resin coating: Fabrication and experimental characterization. *Journal of the Mechanical Behavior of Materials*, 27(5–6).
- Verma, A., Kumar, R., & Parashar, A. (2019). Enhanced thermal transport across a bi-crystalline graphene–polymer interface: An atomistic approach. *Physical Chemistry Chemical Physics*, 21(11), 6229–6237.
- Verma, A., Negi, P., & Singh, V. K. (2018a). Physical and thermal characterization of chicken feather fiber and crumb rubber reformed epoxy resin hybrid composite. *Advances in Civil Engineering Materials*, 7(1), 538–557.
- Verma, A., Negi, P., & Singh, V. K. (2018b). Experimental investigation of chicken feather fiber and crumb rubber reformed epoxy resin hybrid composite: Mechanical and microstructural characterization. *Journal of the Mechanical Behavior of Materials*, 27(3–4).
- Verma, A., Negi, P., & Singh, V. K. (2019). Experimental analysis on carbon residuum transformed epoxy resin: Chicken feather fiber hybrid composite. *Polymer Composites*, 40(7), 2690–2699.
- Verma, A., & Parashar, A. (2017). The effect of STW defects on the mechanical properties and fracture toughness of pristine and hydrogenated graphene. *Physical Chemistry Chemical Physics*, 19(24), 16023–16037.
- Zia, K. M., Jabeen, F., Anjum, M. N., & Ikram, S. (Eds.). (2020). *Bionanocomposites: Green synthesis and applications* Elsevier.
- Wang, T., & Drzal, L. T. (2012). Cellulose-nanofiber-reinforced poly (lactic acid) composites prepared by a water-based approach. *ACS Applied Materials & Interfaces*, 4(10), 5079–5085.
- Xu, Q., Ji, T., Gao, S. J., Yang, Z., & Wu, N. (2019). Characteristics and applications of sugar cane bagasse ash waste in cementitious materials. *Materials*, 12(1), 39.
- Yang, X., He, C., Liu, J., & Diao, H. (2016). Influence on the physical properties of wheat straw via hydrothermal and chemical treatments. *BioResources*, 11(3), 7345–7354.
- Verma, A., Parashar, A., & Packirisamy, M. (2018a). Atomistic modeling of graphene/hexagonal boron nitride polymer nanocomposites: A review. *Wiley Interdisciplinary Reviews: Computational Molecular Science*, 8(3), e1346.
- Verma, A., Singh, V. K., Verma, S. K., & Sharma, A. (2016). Human hair: A biodegradable composite fiber—a review. *International Journal of Waste Resources*, 6(206), 2.
- Verma, A., & Singh, V. K. (2019). Mechanical, microstructural and thermal characterization of epoxy-based human hair–reinforced composites. *Journal of Testing and Evaluation*, 47(2), 1193–1215.

- Verma, A., & Parashar, A. (2018a). Structural and chemical insights into thermal transport for strained functionalised graphene: A molecular dynamics study. *Materials Research Express*, 5(11), 115605.
- Verma, A., Parashar, A., & Packirisamy, M. (2019a). Effect of grain boundaries on the interfacial behaviour of graphene-polyethylene nanocomposite. *Applied Surface Science*, 470, 1085–1092.
- Verma, A., Singh, C., Singh, V. K., & Jain, N. (2019). Fabrication and characterization of chitosan-coated sisal fiber–Phytagel modified soy protein-based green composite. *Journal of Composite Materials*, 53(18), 2481–2504.
- Verma, A., & Singh, V. K. (2016). Experimental investigations on thermal properties of coconut shell particles in DAP solution for use in green composite applications. *Journal of Materials Science and Engineering*, 5(3), 1000242.
- Verma, A., Singh, V. K., & Arif, M. (2016). Study of flame retardant and mechanical properties of coconut shell particles filled composite. *Research and Reviews: Journal of Material Sciences*, 4(3), 1–5.
- Verma, A., Parashar, A., Jain, N., Singh, V. K., Rangappa, S. M., & Siengchin, S. (2020). Surface modification techniques for the preparation of different novel biofibers for composites. In *Biofibers and biopolymers for biocomposites* (pp. 1–34). Cham: Springer.
- Verma, A., & Parashar, A. (2018b). Molecular dynamics based simulations to study the fracture strength of monolayer graphene oxide. *Nanotechnology*, 29(11), 115706.
- Verma, A., Parashar, A., & Packirisamy, M. (2018b). Tailoring the failure morphology of 2D bicrystalline graphene oxide. *Journal of Applied Physics*, 124(1), 015102.
- Verma, A., & Parashar, A. (2018c). Molecular dynamics based simulations to study failure morphology of hydroxyl and epoxide functionalised graphene. *Computational Materials Science*, 143, 15–26.
- Verma, A., Zhang, W., & Van Duin, A. C. (2021). ReaxFF reactive molecular dynamics simulations to study the interfacial dynamics between defective h-BN nanosheets and water nanodroplets. *Physical Chemistry Chemical Physics*, 23(18), 10822–10834.
- Verma, A., Parashar, A., & Packirisamy, M. (2019b). Role of chemical adatoms in fracture mechanics of graphene nanolayer. *Materials Today: Proceedings*, 11, 920–924.
- Verma, A., & Parashar, A. (2020). Characterization of 2D nanomaterials for energy storage. In *Recent advances in theoretical, applied, computational and experimental mechanics* (pp. 221–226). Singapore: Springer.
- Verma, A., Parashar, A., Singh, S. K., Jain, N., Sanjay, M. R., & Siengchin, S. (2020). Modeling and simulation in polymer coatings. In *Polymer coatings: Technologies and applications* (pp. 309–324). Boca Raton: Taylor & Francis Group (CRC Press) (Chapter 16).